Advances in Robotics Research, *Vol. 2, No. 2 (2018) 113-127*
DOI: https://doi.org/10.12989/arr.2018.2.2.113

ROS-based control for a robot manipulator with a demonstration of the ball-on-plate task

Khasim A. Khan[a], Revanth R. Konda[b] and Ji-Chul Ryu[*]

Department of Mechanical Engineering, Northern Illinois University, DeKalb, IL 60115, U.S.A.

(Received December 5, 2017, Revised March 27, 2018, Accepted April 12, 2018)

Abstract. Robotics and automation are rapidly growing in the industries replacing human labor. The idea of robots replacing humans is positively influencing the business thereby increasing its scope of research. This paper discusses the development of an experimental platform controlled by a robotic arm through Robot Operating System (ROS). ROS is an open source platform over an existing operating system providing various types of robots with advanced capabilities from an operating system to low-level control. We aim in this work to control a 7-DOF manipulator arm (Robai Cyton Gamma 300) equipped with an external vision camera system through ROS and demonstrate the task of balancing a ball on a plate-type end effector. In order to perform feedback control of the balancing task, the ball is designed to be tracked using a camera (Sony PlayStation Eye) through a tracking algorithm written in C++ using OpenCV libraries. The joint actuators of the robot are servo motors (Dynamixel) and these motors are directly controlled through a low-level control algorithm. To simplify the control, the system is modeled such that the plate has two-axis linearized motion. The developed system along with the proposed approaches could be used for more complicated tasks requiring more number of joint control as well as for a testbed for students to learn ROS with control theories in robotics.

Keywords: robot operating system (ROS); robot manipulator; balancing control; ball-on-plate system

1. Introduction

Robotics has been growing past the traditional engineering techniques emerging as a newer field of modern technology that requires various knowledge from mechanical and electrical engineering and computer science. When commercial robots are used, the manufacturers often allow users to access the robots in the form of GUI (Graphical User Interface) or APIs (Application Program Interfaces) are provided for further user-customized functionality.

The GUI provided by manufacturers is often not capable of fully exploiting the abilities of the robot and dealing directly with the APIs may be unwieldly. To overcome these inadequacies, middleware packages have been developed (Quigley *et al*. 2009, Bonarini *et al*. 2014) and one

∗Corresponding author, Assistant Professor, E-mail: jryu@niu.edu
[a]Graudate Student, E-mail: Z1748192@students.niu.edu
[b]Graduate Student, E-mail: Z1807320@students.niu.edu

such package is Robot Operating System (ROS). ROS is an open source middleware package that works between multiple platforms and performs OS-like functionality. Since Quigley *et al*. (2009) first developed ROS with the design goals of "Peer to Peer, Multi-lingual, Tools-based, Thin, Free and Open-sources," it has been widely used as software framework of various types of robotic systems. Meeussen *et al*. (2010) use ROS to provide distributed computation for autonomous door opening of a mobile robot called "PR2." For the same mobile manipulator system, Hornung *et al*. (2012) develop a 3D navigation framework based on the Search-Based Planning Library (SBPL) which is part of ROS. Allgeuer *et al*. (2013) implement ROS to a humanoid robot providing visual perception, hardware abstraction, and behavior generation. Aerial robotics is also one of the popular areas in which the software architecture is often built upon ROS. Korpela *et al*. (2012) use ROS to integrate the components of their unmanned aerial vehicle named "MM-UAV." ROS also has a capability that enables the use of other middleware packages along with it. DeMarco *et al*. (2011) integrate MOOS (Mission Oriented Operating Suite), which is popular in the underwater robotics, with ROS to interface different subsystems that are intrinsically difficult to communicate for their autonomous underwater vehicle. From a simple robotic platform such as an Arduino-based mobile robot (Araujo *et al*. 2014) to advanced systems that require high end capabilities like SLAM (Santos *et al*. 2013), ROS has been gaining growing popularity in the robotics community.

The goal of this work is to develop a ROS-based software framework for a manipulator arm which is designed to accomplish complicated tasks. For a demonstration purpose, the task of balancing a ball on a plate has been set on the chosen manipulator arm (Robai Cyton Gamma 300) in this paper. A typical ball and plate system consists of a plate, which has two rotational motions about two perpendicular axes on the plate plane, and a ball, which is placed on the plate and would roll when the plate is tilted under the influence of gravity. This intrinsically nonlinear system has been widely used to demonstrate various control methods. Awtar *et al*. (2002) apply a state-feedback control using the pole placement method to calculate desired angular positions of the plate in the outer loop while a PID controller in the inner loop is designed to achieve the desired angular position. Knuplei *et al*. (2003) use a lead controller with a camera tracking the ball whereas a resistive touch-sensitive glass plate is used to sense the ball position in the work of Awtar *et al*. (2002). Mochizuki and Ichihara (2013) apply I-PD controller, which is a variant of a PID controller, based on generalized Kalman-Yakubovich-Popov (KYP) lemma. Ho *et al*. (2013) apply approximate input-output feedback linearization for each decoupled ball and beam system since the system is not fully feedback linearizable. Nonlinear backstepping control is employed by Wang *et al*. (2008) for the ball-on-plate system along with a switching control in the inner loop of the control structure. Liu *et al*. (2010) design a nonlinear controller based on the sliding mode control technique. Using the proposed controller, trajectory tracking capability is demonstrated in their work. Ghiasi *et al*. (2012) propose a robust optimal controller based on the H-infinity approach to solve a ball trajectory tracking problem under the presence of uncertainties and disturbances. Different approaches to balancing the ball have also been studied such as fuzzy logic (Fan *et al*. 2004), PID neural network (Zheng *et al*. 2011), and fuzzy neural network (Dong *et al*. 2011).

Since most of these previous works rely on a linearized model considering it as two independent ball-on-beam systems while giving satisfactory control performance, the same approach has been adopted in this work. This paper presents the development of a ROS-based software architecture for the chosen manipulator, integrated with a linear control technique and vision tracking system, that demonstrates a task of balancing a ball on a plate. Building on the authors' previous work (Khan and Ryu 2017), in this paper we present satisfactory experimental

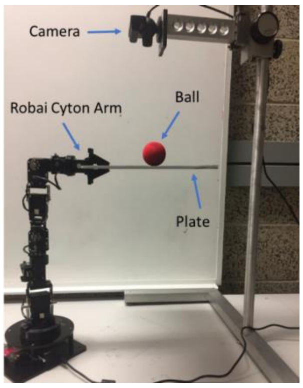

Fig. 1 Experimental setup of the system

results by properly implementing the proposed control scheme.

The rest of the paper is organized as follows: In Section 2, the overview of the developed system is explained. In Section 3, the structure of the designed ROS-based architecture is presented. In Section 4, the derivation of a linearized dynamic model and the design of linear control law are provided. Simulation and experimental results are presented in Section 5, followed by concluding remarks in Section 6.

2. System overview

The system used for the demonstration consists of a 7-DOF robotic arm (Robai Cyton Gamma 300) having 7 servo motors (Dynamixel) as joint actuators, a plate-type end effector, and a vision camera system for tracking. Even though the manipulator has kinematic redundancy with its seven degrees of freedom, only two axes are used as it is sufficient to control the plate for the balancing task. The vision system uses a low-cost USB camera (Sony PlayStation Eye) with frame rates of up to 120 Hz.

As shown in Fig. 1, the plate is held by the gripper of the arm. The plate is given two-axis motion by using two joints of the robot, which is described in more detail in Section 4. For material of the plate and ball, foam and soft rubber were selected respectively, based on the payload limitations of 300 g of the robot arm. Although the model-based control algorithm is designed to work with any mass and size of the ball in principle, a smaller ball was considered to provide enough workspace on the plate along with the payload constraint.

3. System programming with ROS

3.1 Structure of the system software in ROS

ROS is an open-source framework and integrated development environment (IDE) for writing robot software (Quigley *et al*. 2009, Martinez and Fernandez 2013). Since the software interface of the manipulator arm provided by the manufacturer does not give the user complete control over its functionalities, a new software architecture was developed using ROS in this work. This software

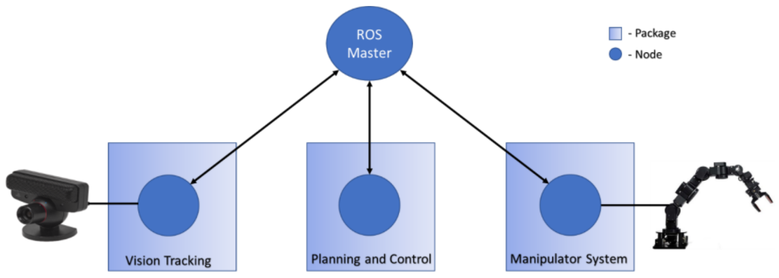

Fig. 2 Employed software architecture of the system in ROS

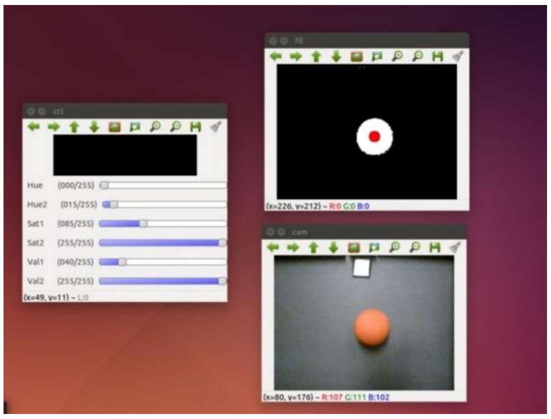

Hue (000/255)
Hue2 (015/255)
Sat1 (085/255)
Sat2 (255/255)
Val1 (040/255)
Val2 (255/255)
(x=49, y=11) ~ L:0

(x=226, y=212) ~ R:0 G:0 B:0

(x=80, y=176) ~ R:107 G:111 B:102

Fig. 3 Image windows of the vision tracking system: (In the clockwise from the left) slide bar control window, tracking-processed image, and original image

architecture makes use of ROS's innate ability to divide the structure into smaller modules that are referred to as "nodes," which have a peer-to-peer communication established between them. For a system which is supposed to conduct complex and dexterous real-world tasks, a divided architecture enabled by software development in ROS provides a few advantages over conventional robot programming: systematic programming procedure, increased code reusability, and structured environment for easier debugging/troubleshooting.

The architecture of the proposed ROS-based system is shown in Fig. 2. At the heart of the architecture is the master node, which makes it possible for nodes to find each other and exchange data. Each node has its own topics and services which can be used to publish or subscribe to messages (Martinez and Fernandez 2013). A node publishes data in a common space under a topic. Other nodes can use this data simultaneously by subscribing to that topic. As shown in Fig. 2, the system has total three programmed packages. The vision system package with a corresponding node therein is for running the camera, tracking the ball, and estimating the position of the ball on the plate. The manipulator system package is for running the joint actuators according to the commanded control input. Due to the open-source nature of ROS, programs and drivers for commonly used components such as Dynamixel motors and USB cameras are available (ROS Wiki 2007). The planning and control package is responsible for taking inputs from the vision system, computing necessary control inputs, and sending the corresponding commands to the manipulator system.

The version of ROS Indigo over Linux OS of Ubuntu Trusty 14.04 was selected to make the best use of pre-developed resources such as the packages for Dynamixel joint actuators and USB cameras.

3.2 Vision tracking system in ROS

A low-cost Sony PlayStation Eye USB camera is mounted above the plate to track the position of the ball as shown in Fig. 1. The object tracking to get the position of the ball is done by a series of image processing steps on grabbed image frames such as image conversion to the HSV color space followed by conversion to grey scale, thresholding, and filtering. OpenCV libraries are used to accomplish the task of tracking a red-colored object (Baggio *et al*. 2012).

The vision tracking system working in multiple windows in Ubuntu OS is shown in Fig. 3. A slide bar control window is created to set the values for HSV, thresholds, and filtering. The PlayStation Eye camera can produce an image frame with a resolution of 320×240 pixels at a frame rate of 120 Hz. Therefore, the camera is strategically mounted on the fixture above the plate of 320×240 mm^2 at a height of 332 mm so that it can cover the entire plate with a position resolution of 1 mm.

3.3 Robai Cyton Gamma 300 with ROS

As mentioned earlier, since the manufacturer of the manipulator arm provides the user with limited control options, the manipulator system package is programmed on top of the Dynamixel package available online (ROS Wiki 2017) to gain complete control over the functionalities of the robot by direct access to the Dynamixel joint actuators. In the implementation, it is important to understand two different control modes available for Dynamixel joint actuators: ‘Joint’ (position) mode and ‘Wheel’ (velocity) mode. Under the joint mode, the Dynamixel joint actuators run based on position inputs with position limits set in the configuration file. On the other hand, under the wheel mode, output velocity is the one to be controlled. In this paper, the wheel mode is selected to be used because the calculated torque input from the control law will be subsequently converted to corresponding velocity input for the arm control, which will be explained in more detail later.

The manipulator system package is created to establish communication from/to the joint actuators. It consists of motor configuration file and related launch files. In this package, two joint controllers were programmed for each of the two joint actuators used for the ball-on-plate task. These joint controllers are for communication with the motors and are different from the controller developed in Section 4.3 for the balancing task. Since, in the proposed demonstration task, only two joint actuators of the 7-DOF manipulator arm need to be controlled in the velocity mode, the other five joints are set to a fixed position as shown in Fig. 1 using the position mode. This is accomplished by first creating a configuration file with the file name extension of ‘yaml’ in which all the necessary parameters are set up. Then a launch file is created to load all the joint controller parameters to the ROS master and start the controllers. A batch file created with the file name extension of ‘sh’ manages moving initially the remaining five joint actuators to a fixed upright position. The joint controllers were programmed so that they send velocity input commands to the two joint actuators which are aligned with the two plate motion axes.

Another important aspect of the Dynamixel joint actuators in using them under ROS is that we can only obtain the position data through the encoder, not the velocity. The angular velocity of the joint actuator can be obtained by numerically differentiating the measured position data through a (digital) low-pass filter.

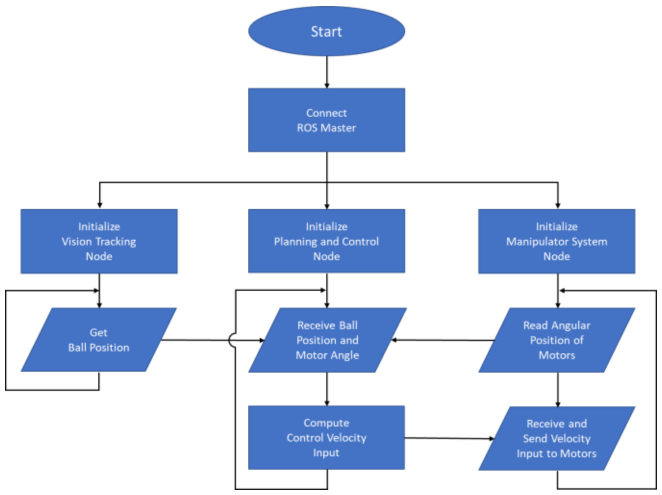
Start
Connect ROS Master
Initialize Vision Tracking Node
Initialize Planning and Control Node
Initialize Manipulator System Node
Get Ball Position
Receive Ball Position and Motor Angle
Read Angular Position of Motors
Compute Control Velocity Input
Receive and Send Velocity Input to Motors

Fig. 4 Flowchart that represents the sequence of operations of the developed, ROS-based software framework for the demonstration task

3.4 Planning and control

The planning and control node brings all the components of the system together and forms a bridge between the vision tracking node and the manipulator system node. It takes in the ball position and the angular joint position data, respectively from the vision tracking system node and the manipulator system node. The ball and angular joint velocities are then calculated through numerical differentiation of the position data. All these measured and calculated values are used to generate appropriate torque inputs to the joint actuators using the linear control law, which will be explained in the next section. Then, this torque input is finally converted to the corresponding velocity input, which will also be explained later, and sent to the manipulator system node. This planning and control node operates at a frequency of 100 Hz.

We represent the sequence of operations of this node, to perform the balancing task, in the form of pseudocode below. The entire sequence of the developed, ROS-based software framework is shown in the flowchart shown in Fig. 4.

```
Pseudocode: Planning and Control Node
    begin
      Subscribe to the topic published by the vision tracking node.
      Subscribe to the topic published by the manipulator system node.
    while (desired state is not acquired) {
        Get the ball position.
        Get the angular position of the motors.
        Calculate the velocities through numerical differentiation and filtering.

        Compute the control torque using the obtained and calculated states
        Integrate the equations of motion to compute the command motor angular velocity.
        Send the command velocity to the motors.
    }
    end
```

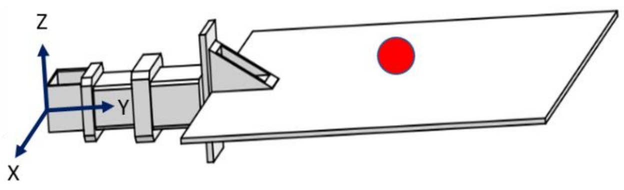

Fig. 5 The coordinate frame used in the system

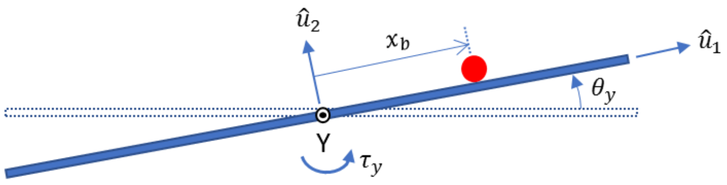

Fig. 6 The Y-axis motion of the system

4. System modeling and control

The ball-on-plate on the robot arm is simplified into two decoupled ball-on-beam systems such that the motion of the ball in each axis is treated as an independent ball-on-beam problem. The ball is assumed to be in contact with the plate at all times under the no-slip assumption.

4.1 Equations of motion

First, the equations of motion of a ball-on-beam is derived using the Lagrangian method (Bolivar-Vincenty and Beauchamp-Baez 2014). The coordinate frame used with the system is shown in Fig. 5.

The two plate motions are rotations about X- and Y-axes. We derive the equations of motion for each rotational motion as below.

About Y-axis:

The parameters of the ball are given by the mass m_b, radius r_b, moment of inertia J_b and the plate by moment of inertia J_p about Y-axis. Then, using the body-attached coordinate frame u_1–u_2 as defined in Fig. 6, the velocity $\tilde{v}_b$ and angular speed ω_y of the ball are written as, respectively, given the position $x_b\hat{u}_1$,

$$\tilde{v}_b = \dot{x}_b\hat{u}_1 + x_b\dot{\theta}_y\hat{u}_2, \qquad \omega_y = \frac{\dot{x}_b}{r_b}$$

We use Euler-Lagrange's equation to derive the equations of motion, with $q = \left[x_b, \theta_y\right]^T$

$$\frac{d}{dt}\left(\frac{\partial L}{\partial \dot{q}}\right) - \frac{\partial L}{\partial q} = \tau \tag{1}$$

where $L = K - V$ and τ denotes the generalized force vector. Here, K and V are the kinetic and potential energies of the system and given by

$$K = \frac{1}{2}m_b v_b^2 + \frac{1}{2}J_b\omega_y^2 + \frac{1}{2}J_p\dot{\theta}_y^2 = \frac{1}{2}\left(m_b + \frac{J_b}{r_b^2}\right)\dot{x}_b^2 + \frac{1}{2}\left(m_b x_b^2 + J_p\right)\dot{\theta}_y^2$$

$$V = m_b g x_b \sin\theta_y$$

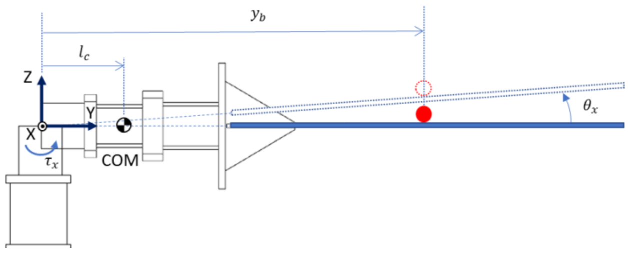

Fig. 7 The X-axis motion of the system

Finally, the equations of motion about Y-axis of rotation are obtained as

$$\left(m_b + \frac{J_b}{r_b^2}\right)\ddot{x}_b - m_b x_b \dot{\theta}_y^2 + m_b g \sin\theta_y = 0 \tag{2}$$

$$(m_b x_b^2 + J_p)\ddot{\theta}_y + 2m_b x_b \dot{x}_b \dot{\theta}_y + m_b g x_b \cos\theta_y = \tau_y \tag{3}$$

where τ_y denotes the torque input on the Y-axis joint.

About X-axis:

The rotational motion about X-axis can also be described as a ball-on-beam system, similar to the motion about Y-axis. However, the critical difference of this motion is the center of mass (COM) of the system is not located at the axis of rotation as shown in Fig. 7. Also, the equilibrium point–the center of the plate–at which the ball is designed to be balanced is not at the axis of rotation, i.e., $y_b \neq 0$ at the balanced position.

We use again Euler-Lagrange's equation to derive the equations of motion. However, due to the aforementioned differences, compared to the previous case it has additional kinetic and potential energies.

Consequently, the kinetic and potential energies of the system are given by

$$K = \frac{1}{2}m_b v_b^2 + \frac{1}{2}J_b\left(\frac{\dot{y}_b}{r_b}\right)^2 + \frac{1}{2}m_s v_p^2 + \frac{1}{2}J_s\dot{\theta}_x^2$$

$$V = m_b g y_b \sin\theta_x + m_s g l_c \sin\theta_x$$

where m_s and J_s are the mass and moment of inertia of the entire system including the links, gripper, and plate; l_c is the location of the COM measured from the axis of rotation; and v_p is the velocity of the system at the COM, given by $v_p = l_c\dot{\theta}_x$. Finally, we obtain the equations of motion as follows

$$\left(m_b + \frac{J_b}{r_b^2}\right)\ddot{y}_b - m_b y_b \dot{\theta}_x^2 + m_b g \sin\theta_x = 0 \tag{4}$$

$$(m_b y_b^2 + J_s + m_s l_c^2)\ddot{\theta}_x + 2m_b y_b \dot{y}_b \dot{\theta}_x + (m_b y_b + m_s l_c) g \cos\theta_x = \tau_x \tag{5}$$

4.2 Linearization around the center of the plate

The objective of the proposed demonstration is to balance the ball at the center of the plate. Assuming the rotation angles θ_x and θ_y are small, the control problem becomes simpler by further applying approximation linearization for the equations of motions in Eqs. (2)-(5).

About Y-axis:

Eqs. (2) and (3), which describes the motion about Y-axis, can be represented in the state space form with $z = \left[x_b, \theta_y, \dot{x}_b, \dot{\theta}_y\right]^T$

$$\dot{z} = f(z, \tau_y) = \begin{bmatrix} \dot{x}_b \\ \dot{\theta}_y \\ -\frac{5}{7} g \sin\theta_y + \frac{5}{7} x_b \dot{\theta}_y^2 \\ \frac{1}{m_b x_b^2 + J_p}\left(-2 m_b x_b \dot{x}_b \dot{\theta}_y - m_b g x_b \cos\theta_y + \tau_y\right) \end{bmatrix}$$

Note that we assume the mass of the ball is uniform, so the moment of inertia of the ball $J_b = \frac{2}{5} m_b r_b^2$. This system is linearized about an equilibrium point $z^* = \left[x_b^*, \theta_y^*, \dot{x}_b^*, \dot{\theta}_y^*\right]^T = [0, 0, 0, 0]^T$and $\tau_y^* = 0$. By the linearization method (Benaroya and Nagurka 2010), the system is now given by

$$\dot{z} = Az + B\tau_y \tag{6}$$

where

$$A = \left.\frac{\partial f}{\partial z}\right|_{z^*, \tau_y^*} = \begin{bmatrix} 0 & 0 & 1 & 0 \\ 0 & 0 & 0 & 1 \\ 0 & -\frac{5}{7} g & 0 & 0 \\ -\frac{m_b g}{J_p} & 0 & 0 & 0 \end{bmatrix}, \quad B = \left.\frac{\partial f}{\partial \tau_y}\right|_{z^*, \tau_y^*} = \begin{bmatrix} 0 \\ 0 \\ 0 \\ \frac{1}{J_p} \end{bmatrix}.$$

Alternatively, Eq. (6) can be expressed in terms of x_b and θ_y.

$$\ddot{x}_b + \frac{5}{7} g \theta_y = 0 \tag{7}$$

$$J_p \ddot{\theta}_y + m_b g x_b = \tau_y \tag{8}$$

About X-axis:

Similarly, we can approximately linearize Eqs. (4)-(5) around the center of the plate which is given by $z^* = \left[y_b^*, \theta_x^*, \dot{y}_b^*, \dot{\theta}_x^*\right]^T = [y_b^*, 0, 0, 0]^T$ and $\tau_x^* = (m_b y_b^* + m_s l_c) g$. Notice that the equilibrium point of y_b^* is not zero in this case since the equilibrium point is off the axis of rotation by y_b^* as can be seen in Fig. 7. Consequently, the equilibrium torque τ_x^* is not zero either.

The equations of motion in Eqs. (4) and (5) can also be rewritten in the state space form with $z = \left[y_b, \theta_x, \dot{y}_b, \dot{\theta}_x\right]^T$as

$$\dot{z} = f(z, \tau_x) = \begin{bmatrix} \dot{y}_b \\ \dot{\theta}_x \\ -\frac{5}{7} g \sin\theta_x + \frac{5}{7} y_b \dot{\theta}_x^2 \\ \frac{1}{m_b y_b^2 + J_s + m_s l_c^2}\left(-2 m_b y_b \dot{y}_b \dot{\theta}_x - (m_b y_b + m_s l_c)\cos\theta_x + \tau_x\right) \end{bmatrix}$$

Due to the nonzero equilibrium point, the approximation linearization yields

$$\dot{\Delta z} = A\Delta z + B\Delta\tau_x \tag{9}$$

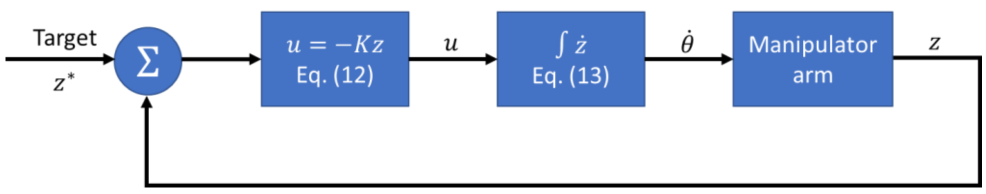

Fig. 8 Schematic of the feedback control loop

where

$$\Delta z = z - z^*, \qquad \Delta\tau_x = \tau_x - \tau_x^*,$$

$$A = \left.\frac{\partial f}{\partial z}\right|_{z^*,\tau_x^*} = \begin{bmatrix} 0 & 0 & 1 & 0 \\ 0 & 0 & 0 & 1 \\ 0 & -\frac{5}{7}g & 0 & 0 \\ -\frac{m_b g}{m_b y_b^* + J_s + m_s l_c^2} & 0 & 0 & 0 \end{bmatrix}, \text{ and } B = \left.\frac{\partial f}{\partial \tau_x}\right|_{z^*,\tau_x^*} = \begin{bmatrix} 0 \\ 0 \\ 0 \\ \frac{1}{m_b y_b^* + J_s + m_s l_c^2} \end{bmatrix}.$$

Alternatively,

$$\ddot{y}_b + \frac{5}{7} g\theta_x = 0 \tag{10}$$

$$(m_b y_b^* + J_s + m_s l_c^2)\ddot{\theta}_x + m_b g(y_b - y_b^*) = \tau_x \tag{11}$$

4.3 Controller design

In this section, we discuss the controller design based on the linearized equations of motion in Eqs. (6) and (9). The well-known linear control technique of the pole placement method is used such that

$$\tau = -Kz \tag{12}$$

where τ denotes the torque control input, z the full state feedback, and K the 1×4 gain matrix given by $K = [K_1\ K_2\ K_3\ K_4]$. With this form of control law, the equations of motion can be rewritten as

$$\dot{z} = (A - BK)z \tag{13}$$

Stabilization to the equilibrium point is guaranteed by determining the gain matrix K in a way that $(A - BK)$ is a Hurwitz.

It should be mentioned that in practice the Cyton Gamma manipulator does not allow torque inputs, but velocity inputs. Hence, we use an approach of numerically integrating the equations of motion with the calculated torque input in Eq. (12) over one control loop interval in order to estimate the target velocity at the next control step. Then, we use the calculated target velocity as the input to the manipulator at the current control step. The schematic of the full state feedback control loop is provided in Fig. 8.

5. Simulation and experimental results

The values of the system parameters used in the simulation and experiment are listed in Table 1.

Table 1 System parameter values used in simulation and experiment

System Parameters	Variables	Actual Values [units]
Mass of the ball	m_b	0.0045 [kg]
Moment of inertia of the ball	J_b	1.046×10^{-6} [kg·m^2]
Radius of the ball	r_b	0.024 [m]
Mass of the plate*	m_s	0.2124 [kg]
Moment of inertia of the plate* (about Y-axis)	J_p	0.29988×10^{-3} [kg·m^2]
Moment of inertia of the plate* (about X-axis)	J_s	2.41003×10^{-3} [kg·m^2]
Distance to the center of mass (COM) from the rotation of axis	l_c	0.0885 [m]
Distance to the plate center from the rotation of axis	y_b^*	0.23 [m]

*The links, gripper, and plate are all considered in computation of these parameters

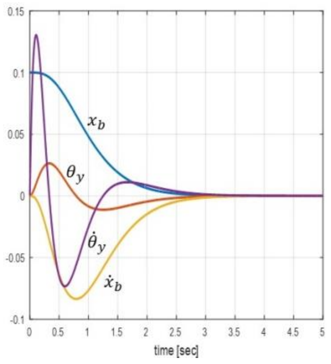

(a) Rotational motion about Y-axis (see Fig. 6)

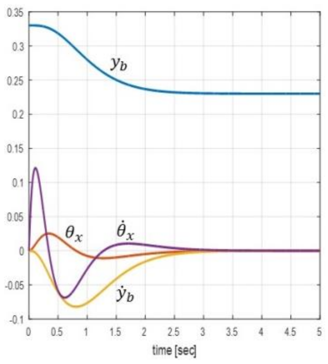

(b) Rotational motion about X-axis (see Fig. 7)

Fig. 9 The simulation results

Since the rotating links, which are considered to be part of the plate, are irregularly shaped, the moment of inertia and COM (see Fig. 7) of the links were determined using a model developed on a CAD software, SOLIDWORKS.

5.1 Simulation results

In the application of the pole placement method, the gain matrix K in Eq. (12) was chosen as $K = [-0.0522, 0.0251, -0.0088, 0.0045]$ and $K = [-0.1820, 0.4278, -0.1505, 0.0766]$ for the rotational motion about Y-axis and X-axis, respectively. These are the cases when the poles of the closed-loop system in Eq. (13) are both at $(-3, -3.5, -4, -4.5)$.

Fig. 9 shows the simulation results. The initial conditions are $(x_b, \theta_y, \dot{x}_b, \dot{\theta}_y) = (0.1\ \text{m}, 0, 0, 0)$ and $(y_b, \theta_x, \dot{y}_b, \dot{\theta}_x) = (0.33\ \text{m}, 0, 0, 0)$, respectively. Note that the initial condition of $y_b(0) =$

0.33 m implies the ball is to be at 0.1 m from the center of the plate. As expected, the ball is stabilized to the center of the plate where $(x_b^*, y_b^*) = (0, 0.23)$ with eventual zero velocity of the ball.

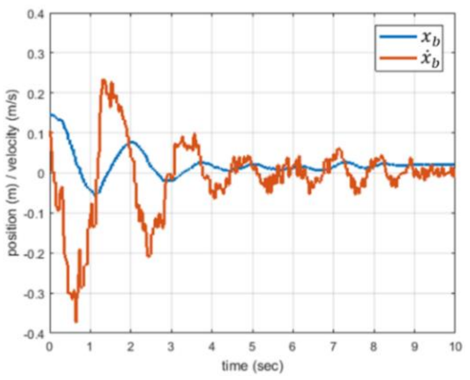

(a) The position and velocity of the ball

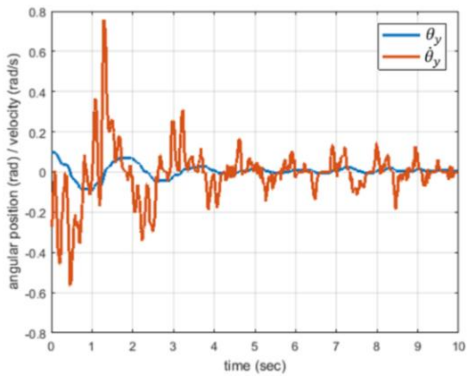

(b) The angular position and velocity of the joint

Fig. 10 The experimental results of the motion about Y-axis

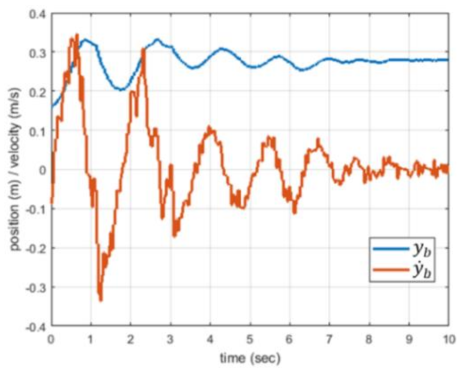

(a) The position and velocity of the ball

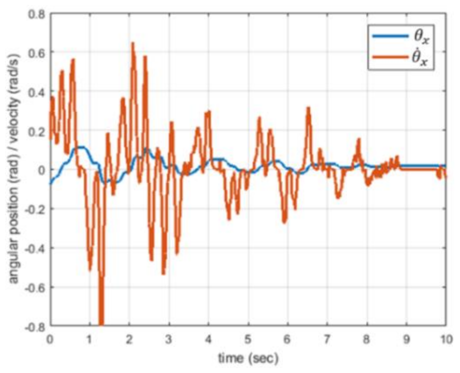

(b) The angular position and velocity of the joint

Fig. 11 The experimental results of the motion about X-axis

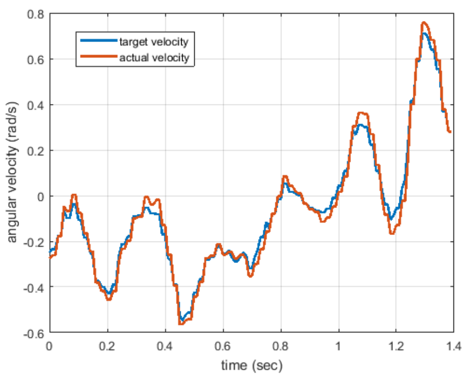

(a) About X-axis

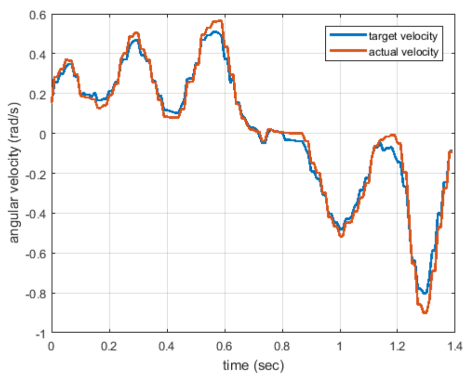

(b) About Y-axis

Fig. 12 The target and actual angular velocities of the joints motors

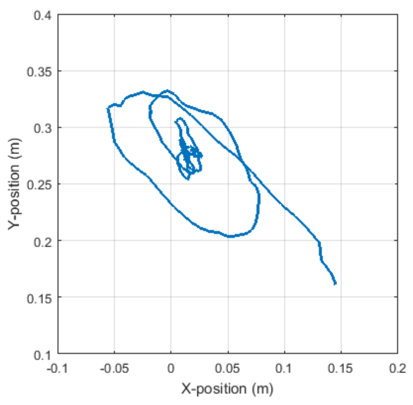

Fig. 13 The trajectory of the ball position on the plate

5.2 Experimental results

As explained in the previous section, the Dynamixel joint motors were set to operate in the velocity mode and the torque control input computed from the control law was converted to corresponding velocity input. In fact, there exists an internal PID control loop running inside the Dynamixel servo motors to achieve the desired velocity output. Since the frequency rate of the internal loop is not sufficiently fast enough, to minimize the effect of it and to enhance the control performance, we added an additional corrective term to the commanded input such that

$$Input = TargetVelocity + K * (TargetVelocity - ActualVelocity)$$

where the additional control gain K was determined as 11.5 (Y-axis) and 13 (X-axis) experimentally.

As Figs. 10 and 11 show, the system performed balancing control satisfactorily and could keep the ball around the center of the plate. Fig. 10 shows the ball and joint motions about Y-axis, described by x_b and θ_y, respectively (see Fig. 6) while Fig. 11 shows the motions about X-axis, by y_b and θ_x, respectively (see Fig. 7). The initial ball position was $\left(x_b(0), y_b(0)\right)$ = (0.14, 0.16) m. It should be mentioned that due to the use of a linearized model in the controller design, stabilization to the equilibrium point, i.e., the center of the plate, is not guaranteed with a large initial offset. Furthermore, it could lead to a system instability.

As observed in the figures, the steady state error of the ball position was (x_{ss}, y_{ss}) = (0.02, 0.05) m. Note that even though the steady state value of y_b reads 0.28 m in Fig. 11, the steady state error y_{ss} in y is 0.05 m because the center plate position is 0.23 m. We consider the control performance is successful if the ball is stabilized, i.e., balanced, to a point within the diameter (0.048 m) of the ball around the center at steady state and the result approximately satisfies the objective. As shown in Fig. 12, the fact that the actual angular velocities follow the targets well shows the validity of the suggested control method in Section 4.3. Fig. 13 shows the trajectory of the ball on the plate during the balancing control. It shows convergence toward the center. The experimental results also show a longer settling time when compared to the simulation results. This is, along with the causes discussed below, in part due to the use of lower control gains to prevent the system from unwanted vibrations caused by overshoot of the joint actuators.

Causes of the existence of the steady state error and longer settling time may include discrepancy between the actual and simplified decoupled dynamics, invalidity of the small angle assumption for the linearized model, delays in image processing and command communication, insufficient control loop rate, and unwanted dynamics introduced by the flexible foam plate chosen due to the payload limitation. It should be mentioned that since the end goal of this work was to program a software framework based on ROS under which a manipulator system could perform various complex tasks, emphasis was not strongly laid on the minimization of the steady state error and the settling time.

6. Conclusions

This paper presents a ROS-based multi-platform interface to control a 7-DOF manipulator arm integrated with a vision tracking system. This system is developed in such a way that the components communicate with each other to receive the state feedback from the vision system and Dynamixel servo motors, and to compute and send control commands to perform prescribed control tasks. For a demonstration purpose, the task of balancing a ball on a plate was performed through simulation and experiment. The experimental results are satisfactory as the system could balance the ball in a small neighborhood of the plate center. The presented system with the proposed approaches could be used for more complicated tasks requiring more number of joint control as well as for a testbed for students to learn ROS programming with control theories in robotics.

References

Allgeuer, P. and Schwarz, M. (2013), "A ROS-based software framework for the NimbRo-OP humanoid open platform", *Proceedings of the IEEE-RAS International Conference on Humanoid Robots*, Atlanta, Georgia, U.S.A., October.

Araújo, A., Portugal, D., Couceiro, M.S. and Rocha, R.P. (2014), "Integrating Arduino-based educational mobile robots in ROS", *J. Intell. Robot. Syst. Theor. Appl.*, **77**(2), 281-298.

Awtar, S., Bernard, C., Boklund, N., Master, A., Ueda, D. and Craig, K. (2002), "Mechatronic design of a ball-on-plate balancing system", *Mechatronics*, **12**(2), 217-228.

Baggio, D.L., Emami, S., Escriva, D.M., Levgen, K., Mahmood, N., Saragih, J. and Shilkrot, R. (2012), *Masterinng OpenCV with Practical Computer Vision Projects,* Packt Publishing, Birmingham, U.K.

Benaroya, H. and Nagurka, M.L. (2010), *Mechanical Vibration: Analysis, Uncertainties, and Control,* CRC Press, Boca Raton, Florida, U.S.A.

Bolívar-Vincenty, C.G. and Beauchamp-Báez, G. (2014), "Modelling the ball-and-beam system from Newtonian mechanics and from Lagrange methods", *Proceedings of 12th Latin American and Caribbean Conference for Engineering and Technology (LACCEI'2014)*, Guayaquil, Ecuador, July.

Bonarini, A., Matteucci, M., Migliavacca, M. and Rizzi, D. (2014), "R2P: An open source hardware and software modular approach to robot prototyping", *Robot Auton. Syst.*, **62**(7), 1073-1084.

DeMarco, K., West, M.E. and Collins, T.R. (2011), "An implementation of ROS on the Yellowfin autonomous underwater vehicle (AUV)", *Proceedings of the Oceans 2011*, Waikoloa, Hawaii, U.S.A., September.

Dong, X., Zhao, Y., Xu, Y., Zhang, Z. and Shi, P. (2011), "Design of PSO fuzzy neural network control for ball and plate system", *J. Innov. Comput. Inf. Control*, **7(**12), 7091-7103.

Fan, X., Zhang, N. and Teng, S. (2004), "Trajectory planning and tracking of ball and plate system using hierarchical fuzzy control scheme", *Fuzzy Set. Syst.*, **144(**2), 297-312.

Ghiasi, A.R. and Jafari, H. (2012), "Optimal robust controller design for the ball and plate system", *Proceedings of the 9th International Conference on Electronics, Computer and Computation*, Ankara, Turkey, November.

Ho, M.T., Rizal, Y. and Chu, L.M. (2013), "Visual servoing tracking control of a ball and plate system: design, implementation and experimental validation", *J. Adv. Robot. Syst.*, **10**(7), 287.

Hornung, A., Phillips, M., Gil Jones, E., Bennewitz, M., Likhachev, M. and Chitta, S. (2012), "Navigation in three-dimensional cluttered environments for mobile manipulation", *Proceedings of the IEEE International Conference on Robotics and Automation*, St. Paul, Minnesota, U.S.A., May.

Khan, K. and Ryu, J.C. (2017), "ROS-based control of manipulator arm for balancing a ball on a plate", *Proceedings of the ASEE Annual Conference & Exposition*, Columbus, Ohio, U.S.A., June.

Knuplei, A., Chowdhury, A. and Sveeko, R. (2003), "Modelling and control design for the ball and plate system", *Proceedings of the International Conference on Industrial Technology*, Maribor, Slovenia, December.

Korpela, C.M., Danko, T.W. and Oh, P.Y. (2012), "MM-UAV: Mobile manipulating unmanned aerial vehicle", *J. Intell. Robot. Syst. Theor. Appl.*, **65**(1-4), 93-101.

Liu, H. and Liang, Y. (2010), "Trajectory tracking sliding mode control of ball and plate system", *Proceedings of the 2nd International Asian Conference on Informatics in Control, Automation and Robotics*, Wuhan, China, March.

Martinez, A. and Fernández, E. (2013), *Learning ROS for Robotics Programming*, Packt Publishing, Birmingham, U.K.

Meeussen, W., Wise, M. and Glaser, S. (2010), "Autonomous door opening and plugging in with a personal robot", *Proceedings of the IEEE International Conference on Robotics and Automation*, Anchorage, Alaska, U.S.A., May.

Mochizuki, S. and Ichihara, H. (2013), "I-PD Controller design based on generalized KYP Lemma for ball and plate system", *Proceedings of the IEEE European Control Conference*, Zurich, Switzerland, July.

Quigley, M., Berkey, B., Conley, K., Faust, J., Foote, T., Leibs, J., Berger, E., Wheeler, R. and Ng, A. (2009), "ROS: An open-source Robot Operating System", *Proceedings of the ICRA Workshop on Open Source Software*, Kobe, Japan, May.

ROS Wiki (2007), *Dynamixel Motor; Robot Operating System (ROS)*, <http:/wiki.ros.org/dynamixel_motor>.

Santos, J.M., Portugal, D. and Rocha, R.P. (2013), "An evaluation of 2D SLAM techniques available in Robot Operating System", *Proceedings of the IEEE International Symposium on Safety, Security, and Rescue Robotics*, Linkoping, Sweden, October.

Wang, H., Tian, Y., Fu, S. and Zhen, S. (2008), "Nonlinear control for output regulation of ball and plate system", *Proceedings of the 27th Chinese Control Conference*, Junming, China, July.

Zheng, F., Li, X., Qian, X. and Wang, S. (2011), "Modeling and PID neural network research for the ball and plate system", *Proceedings of the International Conference on Electronics, Communications and Control*, Ningbo, China, September.

CC